PCCP

Physical Chemistry Chemical Physics

Accepted Manuscript

This article can be cited before page numbers have been issued, to do this please use: A. Ali, R. Kumar , M. A. Iquebal , S. Jaiswal , D. Kumar and A. U. Khan, *Phys. Chem. Chem. Phys.*, 2019, DOI: 10.1039/C9CP02734C.

View Article Online
DOI: 10.1039/C9CP02734C

Role of conserved residues in catalytic activity of NDM-1: an approach of site directed mutagenesis and molecular dynamics

Abid Ali[1], Rakesh Kumar[2], Mir Asif Iquebal[2], Sarika Jaiswal[2] and Dinesh Kumar[2] and Asad U Khan[1]*

1- Medical Microbiology and Molecular Biology Lab, Interdisciplinary Biotechnology Unit, Aligarh Muslim University, Aligarh 202002s, India.

2- ICAR-Indian Agricultural Statistics Research Institute (IASRI), Library Avenue, PUSA, New Delhi -110012, INDIA

Running title: Generation of Mutants in NDM-1

Corresponding author*: Prof. Asad U. Khan, Medical Microbiology and Molecular Biology Lab., Interdisciplinary Biotechnology Unit, Aligarh Muslim University, Aligarh – 202002,UP, India. Ph.: 0091-9837021912, Fax: 0091-571-2721776

Email id: asad.k@rediffmail.com

Key word

NDM-1, Mutant, Antibiotics resistance, Carbapenemase and residues.

View Article Online
DOI: 10.1039/C9CP02734C

Abstract

Rise of New Delhi Metallo Beta-Lactamase-1 (NDM-1) producers is a major public health concerns due to carbapenems resistance. The infection caused by carbapenem-resistant enterobacteria (CRE) is being classified as serious problem. To understand structural and function of NDM-1, amino acid replacement approach is considered as one of the methods to get structural insight. Therefore, we have generated novel mutation (N193A, S217A, G219A and T262A) near active site and omega-like loop to know the role of conserved residues of NDM-1. The minimum inhibitory concentration (MIC) of ampicillin, imipenem, meropenem, cefotaxime, cefoxitin and ceftazidime for all mutants as compared to wild type NDM-1 producing strain, were found reduced by 2 to 6 fold. The Km values were increased while Kcat and Kcat/Km values were decreased as compared to wild type. The affinity as well catalysis properties of these mutants were reduced considerably for imipenem, meropenem, cefotaxime, cefoxitin, ceftazidimem as compared to wild type, hence the catalytic efficiency (Kcat/Km) of all mutant enzymes were reduced as owing to the poor affinity of enzyme. IC50 values of these mutants with each drug was reduced as compared to wild type NDM-1. MD simulation and docking results of mutant protein models along with wild type, showed stable and consistent behavior of RMSD, RMSF and Rg. The α-helices contents of all mutant proteins were reduced by 13%, 6%, 14 % and 9% as compared to NDM-1, Hence, it reveals an imperative role of near active site residues in the enzyme catalytic activity of NDM-1.

View Article Online
DOI: 10.1039/C9CP02734C

1. Introduction:

The World Health Organization (WHO) announced that antibacterial resistance is one of the leading health problems [1]. The usage of antibiotics for the treatment of infectious diseases has been common and effective exercise since decades [2]. However, due to misuse and exploitation of antibiotics, multi-drug resistant bacteria, such as Enterobacterial species may lead a threat to human health. It is quite difficult to control such infection due to the acquirement of numerous resistance mechanisms, including production of extended spectrum β-lactamases and carbapenemases [3,4]. Increasing carbapenem resistance can be recognized by various factors such as acquiring of newer resistance markers and their spread among the bacteria through horizontal gene transfer, increased use of carbapenems, simultaneous dosage of other antibacterial classes and global traveling and migrations [5]. A total of 29 MBLs have been known so far. These are classified on the basis of primary amino acid sequence and function in three sub class (B1, B2 and B3) [6,7]. The subclass B1 includes IMP (imipenamase), VIM (Verona integrin-encoded MBLs) and NDM (New Delhi MBL), each of the markers carries multiple variants [8]. After the discovery NDM-1 in 2008, the worldwide spread of NDM-1 variants has been reported in member of entrobacteriaces members [9,10]. In the sequence of NDM-1, NDM-4, VIM-2, VIM-4 and IMP, the conserved sequence alignment of amino acids residues threonine (T), glycine (G), asparagus (N) and serine (S) are directly involved in tight binding interaction with antibiotics or other substrates as shown in figure.1[5]. NDM-1, IMP 1 and VIM-1 have asparagine, serine, glycine and threonine at the position 193, 217, 219 and 262, respectively, which predicts the evolutionary resemblance among MBLs to understand the importance of such residues near the active site and its catalytic reactions (Figure 2). Presence of threonine (T), glycine (G),

View Article Online
DOI: 10.1039/C9CP02734C

asparagine (N) and serine (S) residues near the omega-loop of serine beta-lactamases has been confirmed to confer hydrolytic reactions by insulating water molecules at the active site for the final deacylation reactions [11,12]. These residues are present at the junction of an alpha helix and a loop near the active site. Four substitutions were made near the zinc-binding active site at the position asparagine 193(N193), serine 217(S217), glycine 219(G219) and threonine 262 (T262) of NDM-1 with alanine to understand the significance of these residues in resistance development. We used alanine residues for the replacement of each mutant because alanine does not eliminate the side chain beyond the β carbon without altering the main-chain conformation nor it does impose extreme electrostatic or steric effects [13]. In addition, we analyzed changes in specific position of selected mutants (N193A, S217A, G219A and T262A) with the wild type to evaluate the effect of mutation on antibiotic susceptibility, enzyme activity and thermal stability.

2. MATERIALS AND METHODS

2.1 Plasmids and bacterial strains

Plasmid DNA harboring $bla_{\text{NDM-1}}$ isolated from *Klebsiella pneumonia* clinical isolates and cloned in the *E. coli DH5α* cells. $bla_{\text{NDM-1}}^{\text{N193A}}$, $bla_{\text{NDM-1}}^{\text{S217A}}$, $bla_{\text{NDM-1}}^{\text{G219A}}$ and $bla_{\text{NDM-1}}^{\text{T262A}}$ mutant clones were made by PCR-based site-directed mutagenesis method using specific primer for each mutation (supplementary table S1) and overexpressed recombinant protein with 0.5mM *IPTG* induction *in E. coli BL21 (λDE3)* cells. MICs of all clones of *E. coli DH5α* cells were measured. Plasmids PQE-2 was used for cloning.

2.2 Reagents and antibiotics

View Article Online
DOI: 10.1039/C9CP02734C

Ampicillin, cefotaxime, cefoxitin, imipenem, meropenem and aztreonam were purchased from Sigma (St. Louis, MO, USA) while nitrocefin was purchased from Calbiochem (USA). Isopropyl-β-D thiogalactopyranoside (IPTG) was purchased from Roche (Basel, Switzerland). All culture media were purchased from Hi-media (Mumbai, India).

2.3 Cloning, mutagenesis, expression and purification

Cloning, mutagenesis, expression and purification of the mutant enzymes (NDM-1^{N193A}, NDM-1^{S217A}, NDM-1^{G219A} and NDM-1^{T262A}) as well NDM-1 were performed using method as described previously, primer list in supplementary Table (S1) [14, 15].

2.4 Antibiotic susceptibility test

MICs were determined in *DH5α* harboring *bla*$_{NDM-1}$ and its mutants (*bla*$_{NDM-1}^{N193A}$, *bla*$_{NDM-1}^{S217A}$, *bla*$_{NDM-1}^{G219A}$ and *bla*$_{NDM-1}^{T262A}$) by broth micro-dilution method as per CLSI guidelines [16].

2.5 Determination IC50 value

The IC50 is the concentration of an inhibitor (Drug) where the response (or binding) is reduced by half. IC50 value was determined by the direct competition between beta-lactamase enzyme with substrate nitrocefin and their inhibitors (drug) under appropriately controlled experiments. Different concentrations of drug (imipenem, meropenem, cefotaxime, cefoxitin and ceftazidime) were taken in increasing order (0 to 3 μM). Fixed concentration of purified protein of NDM-1 and mutants (N193A, S217A, G219A and T262A) were 1nM. Nitrocefin substrate (100 μM) were used in all experiment separately. The rate of hydrolysis of nitrocefin was monitored by the change in absorbance due to cleavage of β-lactam ring at 486 nm using Shimadzu UV-VIS Spectrophotometer UV-1800. The IC50 values were obtained by plotting percent residual enzyme activity on nitrocefin (%) versus inhibitor concentration (log_{10}). The 50% inhibitory

View Article Online
DOI: 10.1039/C9CP02734C

concentration (IC50) was defined as the concentration of the inhibitor that inhibited hydrolytic activity of the enzyme by 50% [17].

2.6 Steady-state enzyme kinetics

Steady-state enzyme kinetic was performed by observing the initial velocities of appearance or disappearance of chromophores of the following antibiotics: nitrocefin (Δε486 = +15,000 M-1 cm-1), ampicillin (Δε235 = -900 M-1 cm-1), cefotaxime (Δε264 = − 7,250 M-1 cm-1), cefoxitin (Δε270 = − 8,380 117 M-1 cm-1), imipenem (Δε295 =− 11,500 M-1 cm-1), meropenem (Δε297 = -10,940 M-1 cm-1) and aztreonam (Δε318 = − 660 M-1 cm- 1). All the experiments were carried out in 50 mM HEPES buffer (pH 7.0) containing 250 mM NaCl and 100 µM ZnCl2 at the 30°C. BSA (20 µg/ml) was added in the dilution buffer to prevent denaturation of NDM-1, N193A, S217A, G219A and T262A mutants enzyme. Initial velocities were calculated and fitted to the Michaelis-Menten equation to calculate the kinetic parameters (Kcat and Km) using equation 1 and 2. Every kinetic value is the mean of three different measurements; the error was recorded below 5%.

$$V = \frac{V_{MAX}\,[S]}{K_M + [S]} \qquad \ldots.1$$

$$V = \frac{V_{MAX}}{[E]} \qquad \ldots.2$$

Where V and Vmax are the initial and maximum velocities, respectively, [s] is the substrate concentration, and [E] is the enzyme concentration as described previously [14,15].

2.7 Structural modelling and molecular dynamics simulation

Tertiary structure of wild type NDM-1 (New Delhi Metallo-β-lactamase-1) was taken from PDB (https://www.rcsb.org/) [18,19]. Mutants (G219A, N193A, S217A and T262A) were constructed

View Article Online
DOI: 10.1039/C9CP02734C

through homology modeling by using same template (NDM) with modeller9v17 [20]. Selection of best models were chosen on the basis of lowest DOPE (Discrete Optimized Protein Energy) score. Newly constructed models along with wild type structure were further optimized through molecular dynamics (MD) simulation.

Molecular dynamics simulations were performed for all the protein models (wild type, G219A, N193A, S217A and T262A) using Groningen Machine for Chemical Simulation (GROMACS 5.0) suite [21]. Protein topology for all the proteins was derived from GROMOS53A6 force field [22]. Each protein system was solvated with the extended simple point charge (SPC/E) water model in cubic box of 1.0 nm distance from the protein to the surface of the box under the given periodic boundary conditions. Each system was neutralized by adding sodium and chlorides ions followed by energy minimization with steepest descent integrator method. After that systems were equilibrated by constant temperature of 300K for 100 ps and pressure of 1 bar for 500 ps. Temperature and pressure of the systems were maintained by Berendsen and Parinello-Rahman methods, respectively. Van der Waals and electrostatic interactions were handled through Lennard-Jones potential and Particle Mesh Ewald (PME) calculation, respectively. All bonds were constrained by using LINCS algorithm [23]. Finally, 50 ns production run was carried by applying 2 fs time step and 2 ps final coordinated were saved. All MD simulation analyses were performed using gmx energy, gmx rms, gmx rmsf and gmx gyrate modules of GROMACS utility.

2.8 Structure validation and molecular docking

Structure validation of all the protein models was accomplished by using different quality check tools. Initially, the models were validated through the inspection of phi/psi distribution by plotting in Ramachandran plot obtained from PROCHECK analysis using SAVES (Structure

View Article Online
DOI: 10.1039/C9CP02734C

Analysis and Verification Server) server (http://servicesn.mbi.ucla.edu/SAVES/) [24]. Further, qualities of all the models were examined through ERRAT and Verify 3D programs of SAVES server and ProSA (Protein Structural Analysis) web server [25, 26]. Refined protein models were further used for molecular docking.

Molecular docking was carried by using Autodock Vina software [27]. Molecular structure of drugs (Imipenem and Meropenem) were downloaded from Drugbank (https:www. drugbank.com) [28] and 3D coordinates were derived from Open Babel tool [29]. Prior to docking, both receptors or proteins and ligands or drugs were prepared in Auto Dock tools [30]. Receptors were prepared by adding polar hydrogens and merging non-polar hydrogens and ligands were prepared by adding Gasteiger charges. Binding site of the ligand was taken from the available protein-ligand complex in PDB (PDB Id:5YPI) and used as a reference to set the dimensions of grid box in current receptor molecules [19]. A grid box of 28, 28, 28 points of dimensions with x, y, z coordinates (-4.903, 13.284, 21.541) were setup in order to cover the active residues in the binding site of the protein. A constant or same configuration and dimensions of grid box was set for all protein-ligand systems (wildtype and mutants) in order to evaluate the docking scores of all protein-drug complexes. Each receptor and ligand were saved in pdbqt format and finally docked in Vina tool. Open Babel tool was employed for the conversion of pdbqt to pdb format. Best binding pose of each receptor-ligand complex were selected as input for MD simulation.

2.9 MD simulation and assessment of protein-drug binding energies.

The complexes of wild type, G219A, N193A, S217A and T262A bound to imipenem and meropenem drugs were selected as started conformation for MD simulation. MD simulation was carried out using GROMACS 5.0. Protein and ligand topologies were derived using GROMOS53A3 force field and PRODRG sever [31], respectively. Procedure of MD used for

View Article Online
DOI: 10.1039/C9CP02734C

protein-ligand complexes were same as used in above case and MD simulation was ran 50 ns for each protein-ligand complex. Binding energies of protein-ligand complexes were calculated by using MM-PBSA (Molecular Mechanics– Poisson Boltzmann Surface Area) method as described previously [7]. Initially, protein-ligand interaction energy was calculated in GROMACS using equation 3.

$$E_{Int} = < E_{LJ} > \; + \; E_{Coul} \qquad \ldots 3$$

E_{Int} is the interaction energy calculated by the short-range Lennard-Jones E_{LJ} and Coulomb energy E_{Coul}.

Later, binding energy was calculated by using g_mmpbsa module of GROMCAS [32] as given in equation 4

$$\Delta G_{binding} = G_{complex} - (G_{protein} + G_{ligand}) \qquad \ldots 4$$

Where $G_{complex}$ is the total free energy of the protein-ligand complex and $G_{protein}$ and G_{ligand} are the total free energies of the proteins and ligands alone. In this study, the binding free energy of the protein-ligand complexes were measured from last stable 20 ns period of MD simulation analyses.

Root mean square deviation (RMSD), root mean square fluctuation (RMSF), radius of Gyration (Rg), hydrogen bond formation (H-bond) of protein-drug complexes were calculated using gmx rms, gmx rmsf, gmx gyrate and gmx hbond modules of GROMACS utility, respectively. Secondary structures formation during MD simulation was calculated from do_dssp module. All 2D and 3D maps of protein-ligand complexes were depicted in LigPlot+ [33] and PyMOL (The PyMOL Molecular Graphics System, Version 1.3 Schrodinger, LLC), respectively. All tertiary

View Article Online
DOI: 10.1039/C9CP02734C

models for visualization were analyzed and displayed in PyMOL. Graphs were plotted using MS Excel and Grace tools.

2.10 Far UV-CD spectra measurement

The far-UV CD spectra of NDM-1 and NDM-1 ^{G219A} , NDM-1 ^{N193A} , NDM-1^{S217A} and NDM-1^{T262A} mutants were recorded on Jasco J-815 spectropolarimeter (Jasco International, Tokyo, JAPAN) equipped with a Peltier-type temperature controller (PTC-423S/15) (17). The enzyme concentration and path length used in the reaction were 5μM and 0.1cm, respectively. The observed ellipticity (θ_{obs} in degree) was converted to mean residue ellipticity (MRE) in degrees per square centimeter per deci mole using the eqution 5 and 6.

$$\mathrm{MRE} = \frac{\theta \mathrm{obs}}{10 \times \mathrm{n} \times \mathrm{c} \times \mathrm{l}} \qquad \ldots 5$$

C is the molar concentration of protein, n is the number of amino acid residues, and l is the path length (in centimeters) and θobs is the observed ellipticity (in degrees).

$$\%\,\alpha\ -\mathbf{helix} = \left(\frac{\mathrm{MRE\ 222nm} - 2340}{30300}\right)100 \qquad \ldots 6$$

MRE value for helical content was calculated at 222 nm. (MRE222) using the fallowing relation as described by Chen et al.

3 RESULTS

3.1 Antibiotic susceptibility test

The *bla*$_{NDM-1}$ and its mutants were cloned and transformed into *E. coli* DH5α cells. These clones (*bla*$_{NDM-1}$ *bla*$_{NDM-1}^{N193A}$, *bla*$_{NDM-1}^{S217A}$, *bla*$_{NDM-1}^{G219A}$ and *bla*$_{NDM-1}^{T262A}$) were used to check the minimum inhibitory concentration with imipenem, meropenem, cefotaxime, cefoxitin and ceftazidime. The MICs of the *bla*$_{NDM-1}$ and all mutants (*bla*$_{NDM-1}^{N193A}$, *bla*$_{NDM-1}^{S217A}$, *bla*$_{NDM-1}^{G219A}$ and *bla*$_{NDM-1}^{T262)}$ were found to be reduced by 2 to 6 fold (Table 1).

View Article Online
DOI: 10.1039/C9CP02734C

3.2 Determination of IC50 Value

The IC50 is the concentration of an inhibitor (Drug) where the response (or binding) is reduced by half. In this study IC50 values for all mutants were calculated and compared to wild type NDM-1 against antibiotics used (imipenem, meropenem, cefoxitin and ceftazidime). All mutants were found to reduce their activity over 50% against these antibiotics a shown the table 2 and figure 3.

3.3 Analysis of the steady state kinetics parameter

The enzyme kinetics was performed using purified NDM-1enzyme and all mutants' enzymes (N193A, S217A, G219A and T262A) with each of the antibiotic (imipenem, meropenem, cefotaxime, cefoxitin, ceftazidime and aztreonam). The enzyme kinetics parameter Km values were increased while Kcat and Kcat/km values were found decreased as compared with the wild type (Table 3). In particular, the affinity of the NDM-1^{N193A}, NDM-1^{S217A}, NDM-1^{G219A} and NDM-1^{T262A} mutants were reduced considerably for imipenem, meropenem, cefotaxime, cefoxitin, ceftazidime, hence the catalytic efficiency (Kcat/Km) of all mutant enzymes were reduced as owing to the poor affinity of the enzyme.

3.4 Construction of tertiary models of the mutant proteins

Initially, *in silico* mutagenesis was accomplished by replacing the targeted amino acid residue with alanine and models were constructed using wild type protein as a template. Homology modeling approach was employed for the construction of tertiary structures of mutant proteins in modeler. It predicted 5 models for each protein and final model was selected on the basis of lowest DOPE score (Figure S1). We found that G219A (Figure S1A) model exhibit DOPE score -28500.313 and energy profile showed similar pattern with the template (Table S2; Figure S1B). DOPE score of N193A models (Figure S1C) was -28339.381 and energy profile of mutant

View Article Online
DOI: 10.1039/C9CP02734C

protein and wild type (template) has similar pattern (Table S2; Figure S1D). DOPE score of S217A model (Figure S1E) was -28385.564 and similar pattern of energy profile was observed in both wild type and S217A mutant protein (Table S2; Figure S1F). Finally, DOPE score of T262A (Figure S1G) model was -28279.77 with similar pattern of energy profile was found with template or wild type protein (Table S2; Figure S1H). Results indicated that all mutant protein tertiary models were showed better DOPE scores and similar energy profiles pattern with the wild type proteins. All models were further optimized by molecular dynamics simulation.

3.5 Molecular dynamics simulations of protein models

Molecular dynamics (MD simulation was used to refine and check the stability of protein models in dynamic system. MD simulation for all protein models were carried about 50 ns of production run and energy, RMSD (root mean square deviation), RMSF (root mean square fluctuation) and Radius of gyration (Rg) were measured (Figure 4). Wild type structure was stabilized at very low value of energy (~ -4.3e+05) followed by energies of N193A (~ -4.15e+05), T262A (~ -4.08e+05), S172A (~ -4.05e+05) and G219A (~ -4.03e+05). Low values of energy for all models indicated that all models were well stabilized (Figure 4A). All models showed consistent behavior of root mean square deviation (RMSD) at different values (Figure 4B). A stable behavior of RMSD of wild type protein was achieved after 10 ns at ~0.23 nm while G219A models showed a consistent behavior of RMSD at an average value ~0.23 nm after 5 ns. N193A model was stabilized an RMSD of ~0.26 nm achieved after 25 ns of simulation time period. S172A and T262A models showed the stable behavior of RMSD at 0.3 nm and 35 nm after 30 and 33 ns, respectively (Figure. 4B). All models showed consistent and stable behavior of RMSD. Mobility of amino acids residue of different proteins were monitored through measuring the root mean square fluctuation (RMSF) (Figure 4C). Wild type and T262A showed stable

View Article Online
DOI: 10.1039/C9CP02734C

behavior of RMSF with no fluctuation except N and C terminal regions of protein which are flanking regions. S217A showed fluctuation at approximately residue number 70 which occupied turn region of the protein and rest of protein model showed stable behavior of RMSF. G219A and N193A models showed stable behavior of RMSF except residue number 150 and 220, respectively showed fluctuation at 0.4-0.5 nm values. Overall value of RMSF for all the models were in the range of 0.2-0.26 nm indicating models were well stabilized with minor fluctuation at turn regions. Globularity and compactness of all the proteins models were examined through measuring the radius of gyration (Rg) (Figure 4D). Compactness of wild type, G219 and N193A models were achieved Rg values of 1.7 nm with consistent behavior after 10 ns of simulation while S217A and T262A showed consistent behavior of Rg after 30 ns of simulation time period at 1.72 and 1.75 nm values. Stable and consistent behavior of Rg indicated all protein models are well compacted. Results obtained from MD simulation indicated that all protein models along with wildtype showed stable and consistent behavior of RMSD, RMSF and Rg.

3.6 Quality assessment and validation

Ramachandran plot was used to depict the phi/psi distribution of all the protein models and observed that 92.6%, 6.9%, and 0.5% of residues of wild type protein were placed in favored, allowed and disallowed regions, respectively (Table S3; Figure S2A). In case of G219A and N193A proteins 94.1%, 4.9%, 1% and 94.1%, 5.4% and 0.5% of residues were placed in favored, allowed and disallowed regions, respectively (Table S3; Figure S2 C and E). Ramachandran plots in case of S217A and T262A proteins, showed 94.6%, 4.9%, 0.5% and 94.1%, 5.4% and 0.5% of residues in favored, allowed and disallowed regions, respectively (Table S3; Figure S2G and I). Larger number of residues was placed in the favored regions suggested that all protein structures are stereo chemically stable. Quality of protein structures

View Article Online
DOI: 10.1039/C9CP02734C

was monitored by ERRAT program and showed that wild type and mutant proteins viz G219A, N193A, S217A and T262A exhibited 93.4, 93.5, 93.9, 90.5 and 94.4% of overall quality (Table S3). VERIFY-3D scores per residue was in the average score of >0.2 for 100% of residues in case of wild type, G219A and N193A, while 99.59% of residues in case of S217A and T262A proteins, respectively (Table S3). Protein structure quality was also examined through Z-score of ProSA web server that displayed the structures to fall in acceptable range of NMR/X-ray studies (Table S3; Figure S2). Z-score of all the models showed in the range of -8.0 to -8.6. Above results showed that all models were stereo chemically and geometrically stable and ready to use for docking.

3.7 Molecular docking and protein-ligand interaction

Docking of wildtype and mutant proteins with imipenem and meropenem drugs were carried in Autodock Vina tool where ligand binding affinity toward receptors was expressed in $\Delta E_{kcal/mol}$ (Table 4). Sampling procedure of drugs for the docking purpose was implement as the default 3D conformation of ligand molecule for all wildtype and mutant-drug complexes. In case of imipenem ligand, Gasteiger charges were added and merged with 2 non-polar hydrogens having 6 aromatic carbon and detected 7 rotatable bonds. While in case of meropenem ligand, Gasteiger charges were added and merged with 2 non-polar hydrogens having 10 aromatic carbon and detected 6 rotatable bonds. Same or default conformations of both imipenem and meropenem ligands were used for all (wildtype and mutants) docking processes. Docking scores of wild type with imipenem and meropenem drugs were -5.9 and -7.1, respectively while drugs namely imipenem and meropenem complexed with G219A showed -5.7 and -7.1 docking scores, respectively. Complex of N193A and imipenem and meropenem drugs showed -5.7 and -7 docking scores, respectively. Docking scores of S217A and T262A complexed with imipenem

View Article Online
DOI: 10.1039/C9CP02734C

and meropenem drugs were -5.8, -7, and -5.9, -7, respectively. G219A-imipenem, N193A-impenem and S217A-imipenem complexes showed less binding affinities as compared to wild type imipenem and T262A-imipenem indicating imipenem drug has more binding affinity toward wild type and T262A as compared to G219A, N193A and S217A. On the other hand, N193A-meropenem, S217A-meropenem and T262A-meropenem complexes showed less binding affinities as compared to wild type meropenem and G219A- meropenem indicating meropenem drug has more binding affinity toward wild type and G219A as compared to N193A, S217A and T262A.

Binding frequency of drugs toward receptors was also monitored by inspection of hydrogen as well as hydrophobic bonds through visualizing the protein-drug complexes in 3D and 2D plots. 3D plots of all protein-drug complex showed that both drugs accommodated well in the pocket surface of receptors (Figure S3A-J). 8 hydrogen bonds were formed between wild type protein and imipenem drug by His120, His122, Gln123, Asp124, Cys208, Lys211, Asn220 and Asp223 residues. Ile35, Trp93, Gly219, Ser217 and His250 residues provide hydrophobic interaction (Figure S3A*). G219A-imipenem complex exhibited 5 hydrogen bonds (His122, Gln123, Asp124, His189, Asp223 and His250) and 8 residues (Ile35, Leu65, Met67, Val73, Trp93, Asn220 and Asp223) provide hydrophobic interactions (Figure S3B*). N193A-imipenem complex also exhibited 5 hydrogen bonds with Asp212, Lys216, Ser217 and Ser251 residues and 7 residues (Ile35, Trp93, Asp124, Lys211, Ala215, Gly219 and His250) were involved in hydrophobic interactions (Figure S3C*). S217A-imipenem complex exhibited 7 hydrogen bonds with His122, Gln123, Asp124, His189, Cys208, Lys211, and Asn220 residues and 4 residues (Ile35, Trp93, Gly219 and His250) were involved in hydrophobic interactions (Figure S3D*). Finally, T262A-imipenem complex exhibited 6 hydrogen bonds with His122, Gln123, Asp124,

View Article Online
DOI: 10.1039/C9CP02734C

His189, Lys211, and Asn220 residues and 5 residues (Ile35, Trp93, Gly219, Cys208 and His250) were involved in hydrophobic interactions (Figure S3E*).

On the other hand, 3 hydrogen bonds (His122, Cys208, Lys211 and Asp223) and 10 hydrophobic interactions (Ile35, Val73, Met67, Trp93, Asp124, Glu152, His189, Gly219, Cys208 and His250) were formed between wild type meropenem complexes (Figure S3F*). G219A-meropenem complex exhibited 5 hydrophilic interactions through His122, Gln123, Asp124, His189 and His250 and 8 hydrophobic interactions through Ile35, Leu65, Met67, Trp93, Cys208, Lys211, Ala219 and Asn220 (Figure S3G*). N193A-meropenem complex exhibited 4 hydrophilic interactions through His122, His189 and His250 and 5 hydrophobic interactions through Met67, Val73, Trp93, Gln123 and Cys208 (Figure S3H*). S217A-meropenem complex exhibited 3 hydrophilic interactions through His122, Cys208 and Lys211 and 10 hydrophobic interactions through Ile35, Met67, Val73, Trp93, Asp124, Glu152, His189, Gly219, Asn220 and His250 (Figure S3I*). Finally, T262A-meropenem complex exhibited 2 hydrogen bonds with His122 and Lys211 residues and 11 residues (Ile35, Met67, Val73, Trp93, Asp124, Glu152, His189, Cys208, Gly219, Asn220 and His250) were involved in hydrophobic interactions (Figure S3J*). Protein-ligand interaction results suggested that all mutant protein-drug complexes were having less capacity of hydrogen bonds formation as compared to wild type protein-drugs complexes with both imipenem and meropenem. However, all mutant protein-drug complexes were mainly stabilized by hydrophobic interactions. Current docking procedure was compared with X-ray structure (PDB ID: 5YPI) available in PDB. RMSD value was calculated by super-imposing the adopted docking procedure and experimentally resolved protein-drug complexes (PDB ID: 5YPI) to validate the present docking results (Figure S4). We

View Article Online
DOI: 10.1039/C9CP02734C

found 0.23Å RMSD value between two docking complexes, showed our docking complex is similar to experimentally resolved protein-ligand complex.

3.8 Molecular dynamics simulation of protein-ligand complexes

Molecular dynamics simulation is routinely using for monitoring the stability of protein-ligand/protein/DNA complexes, to rescoring the binding energy of protein complexes and to study the conformational changes occurring during ligand binding and unbinding[34, 35]. Here, MD simulation is used to check the stability of protein-ligand complexes in dynamic system by means of measuring the RMSD, RMSF and radius of gyration. In addition to that, effect of drugs on the protein secondary structures formation during MD simulation was also carried. RMSD of different proteins (wild type and mutants) with imipenem drug were measured and found that wild types, G219A, N193A and T262A showed consistent behaviors at approximately 0.2, 0.21, 0.25 and 0.23 nm of average RMSD values (Figure 5A). While in case of S217A, RMSD showed consistent behavior in between 10 to 23 ns of simulation period with highly unstable after 23 ns till the end of simulation time. RMSD of different drugs were calculated and found that all drugs showed stable and consistent behavior after 20 ns at low values (0.15 – 0.2 nm) of RMSDs (Figure 5B). Stability of different parts of protein at amino acids level in the presence of drug was monitored by measuring the RMSF (Figure 6A). RMSF of all the proteins showed stable behavior with average values of wild type; G219A, N193A, S217A and T262A were in between 0.1-0.2 nm with minor fluctuations at 70-73 amino acids in case of S217A and at 171 to 174 amino acids in case of wild type with slightly higher RMSF values 0.4 nm. Similar fluctuations of S217A were also observed during receptor alone, indicating that drug has no role during the fluctuation of this segment. While no fluctuations were observed at amino acids of 171-174 in

View Article Online
DOI: 10.1039/C9CP02734C

the wild type protein alone indicating that these amino acids help in binding process of drug. Thus, results of RMSF demonstrated that wild type protein undergoes some conformational changes to accommodate the ligand for making stable complex while imipenem drug has no role or effect on the stabilities of mutant proteins. Further stabilities of different protein-ligand complexes were also monitored by measuring the Rg (Figure. 6B). Rg of all the protein-ligand complexes showed stable and consistent behavior except S217A protein that showed unstable behavior in between and end of the simulations periods. The results of Rg were coincide with the results of RMSD and observed that S217A-impenem complex is less stable.

On the other hand, RMSD of proteins complexed with meropenem drug showed stable behaviors with average RMSD values ranging 0.17 to 0.24 nm (Figure 5C). Wild type-meropenem, G217A-meropenem, N193A-meropenem and T262A-meropenem complexes showed stable behavior of RMSD after 25 ns of simulation period, while S217A-meropenem complex was stabilized after 20 ns with slight deviation at the end of simulation period. RMSD of drug also found to be constant behavior with RMSD values of 0.1-0.2 nm except meropenem complexed with N193A, T262A and S217A displayed deviation in between and end of the simulation time periods (Figure 5C). Similar results were also observed during RMSF in which meropenem complexed with N193A, T262A and S217A showed higher fluctuation at around 245-248 amino acids with 0.5 nm as compared to the rest of proteins where it showed only 0.1-0.2 nm average RMSF values (Figure 6C). While these fluctuations were not observed in receptors without drugs indicating that these amino acids helped in binding of the ligands. Compactness of protein-meropenem complexes were measured through Rg and observed that all complexes displayed consistent and constant values of Rg (1.7 nm) (Figure 6D). The above results indicating that all

View Article Online
DOI: 10.1039/C9CP02734C

protein-meropenem complexes exhibited similar behaviors of RMSD, RMSF and Rg with slight deviation in some mutant-meropenem complexes.

3.9 Secondary structures and H-bond formation during MD simulation

Secondary structures formation such as coil, helices, sheets, turns and bend in wild type and mutant proteins in presence and absence of drugs were examined through DSSP module during MD simulation. Bend and turns formation showed variation which were compensated by corresponding increasing or decreasing the percentage of sheets and helices (Figure 7). Wild type consisted 23%, 26%, 14%, 11% and 24% of coil, β-sheets, bend, turn and α-helices, respectively while in presence of imipenem and meropenem drugs it formed 23%, 26%, 15%, 12%, 23% and 24%, 25%, 16%, 11%, 22% of coil, β-sheets, bend, turn and α-helices, respectively (Figure 7A and B). G219A consisted 23%, 26%, 15%, 12% and 22% of coil, β-sheets, bend, turn and α-helices, respectively while in presence of imipenem and meropenem drugs it formed 23%, 26%, 14%, 12%, 24% and 23%, 25%, 15%, 12%, 22% of coil, β-sheets, bend, turn and α-helices, respectively. N193A consisted 24%, 25%, 14%, 12% and 22% of coil, β-sheets, bend, turn and α-helices, respectively, while in presence of imipenem and meropenem drugs it formed 23%, 27%, 13%, 11%, 24% and 23%, 26%, 13%, 12%, 23% of coil, β-sheets, bend, turn and α-helices, respectively (Figure. 7A and B). S217A consisted 24%, 26%, 15%, 11% and 22% of coil, β-sheets, bend, turn and α-helices, respectively, while in presence of imipenem and meropenem drugs it formed 23%, 26%, 15%, 12%, 21% and 23%, 26%, 15%, 12%, 21% of coil, β-sheets, bend, turn and α-helices, respectively. Finally, T262A consisted 25%, 25%, 13%, 13% and 22% of coil, β-sheets, bend, turn and α-helices, respectively while in presence of imipenem and

View Article Online
DOI: 10.1039/C9CP02734C

meropenem drugs it formed 22%, 27%, 14%, 12%, 23% and 24%, 25%, 14%, 13%, 21% of coil, β-sheets, bend, turn and α-helices, respectively (Figure 7A and B). Results of secondary structure analysis showed that in most of the cases, proteins formed stable secondary structure entities (sheets and helices) in the presence of both the drugs lead to the acquisition of stable complex during MD simulation.

Hydrogen bond (h-bond) formation between proteins and ligands (imipenem and meropenem) were studied by MD simulation through h-bond module of GROMACS. 2-3 h-bonds were observed in the complexes wild type imipenem, G219A-imipenem, N193A-imipenem and T262A-imipenem while 1-2 h-bonds were formed between S217A-imipenem throughout the MD simulation (Figure S5). On the other hand, in case of the protein complex with meropenem drug, 2 hydrogen bonds or sometime 3 h-bonds were formed in case of wild type imipenem, G219A-imipenem, S217A-imipenem and T262A-imipenem, while N193A-imipenem complex exhibited only 2 h-bonds throughout the MD simulation (Figure S6). Above results showed that all protein-drug complexes exhibited almost similar number of h-bonds with slightly more or less in number in some cases during the MD simulation.

3.10 Binding free energy calculation

Rescoring of binding energies were calculated by g_mmpbsa module of GROMACS where trajectories of last 20 ns time period were used to score the binding energy components (Table 5 and 6). Wild type imipenem complex consisted of -64.726, -2.054, 33.695, -8.25 and -41.509 kcal/mol van der Waal's, electrostatic, polar solvation, SASA and binding energies, respectively (Table 5). G219A-imipenem complex consisted of -104.481, -3.842, 34.88, -12.289 and -85.53 kcal/mol van der Waal's, electrostatic, polar solvation, SASA and binding energies, respectively. N193A-imipenem complex consisted of -100.377, -1.817, -21.925, -11.613 and -85.53 kcal/mol

View Article Online
DOI: 10.1039/C9CP02734C

van der Waal's, electrostatic, polar solvation, SASA and binding energies, respectively. S217A-imipenem complex consisted of -70.842, -3.078, 23.863, -7.496 and -57.018 kcal/mol van der Waal's, electrostatic, polar solvation, SASA and binding energies, respectively. And T262A-imipenem complex consisted of -25.877, -1.77, -22.886, -2.891 and -7.66 kcal/mol van der Waal's, electrostatic, polar solvation, SASA and binding energies, respectively. Imipenem complexes with G219A, N193A showed higher binding free energies as compared to imipenem complexed with S217A and wildtype while T262A complex showed very low binding free energies. On the other hand, Wild type meropenem complex consisted of -133.305, -12.908, 52.441, -13.98 and -108.025 kcal/mol van der Waal's, electrostatic, polar solvation, SASA and binding energies, respectively (Table 6). G219A-meropenem complex consisted of -113.925, -10.319, 45.189, -12.551 and -91.735 kcal/mol van der Waal's, electrostatic, polar solvation, SASA and binding energies, respectively. N193A-meropenem complex consisted of -64.023, 0.168, 23.295, -7.658 and -48.468 kcal/mol van der Waal's, electrostatic, polar solvation, SASA and binding energies, respectively. S217A-meropenem complex consisted of -107.628, -0.511, 22.536, -10.635 and -96.577 kcal/mol van der Waal's, electrostatic, polar solvation, SASA and binding energies, respectively. And T262A-meropenem complex consisted of -130.878, -9.63, 44.223, -13.499 and -109.663 kcal/mol van der Waal's, electrostatic, polar solvation, SASA and binding energies, respectively. Meropenem complexes with wildtype and T262A showed almost similar and higher binding energies as compared to meropenem complexed with G219A and S217A, while N193A-meropentttem complex showed lesser binding energy. We found that different mutant exhibited different binding energies both with imipenem and meropenem drugs. Binding energy components suggested that van der Waal's energy were the major contributor for binding of both the ligands.

View Article Online
DOI: 10.1039/C9CP02734C

3.11 Secondary structure analysis

Far-UV CD spectra were utilized to prove the change in the secondary structure of NDM-1 as compared with all mutant NDM-1^{N193A}, NDM-1^{S217A}, NDM-1^{G219A} and NDM-1^{T262A}. The spectrum of NDM-1 and all mutants were similar to the characteristic spectrum of a typical protein rich in α-helix and β sheets with peaks at 218 nm and 222 nm. The MRE at 222 nm was used to calculate the α-helical content by equation 5 and 6. The α-helical contents were found 19.5%, 17.02%, 18.33%, 19% and 18% for NDM-1, NDM-1^{N193A}, NDM-1^{S217A}, NDM-1^{G219A} and NDM-1^{T262A}, respectively. The α-helices contents of NDM-1^{N193A}, NDM-1^{S217A}, NDM-1^{G219A} and NDM-1^{T262A} were reduced by 13%, 6%, 14 % and 9% as compared to NDM-1, respectively (Figure 8).

4 Discussion:

β-lactam antibiotics such as penicillin, cephalosporin and carbapenem, remain to be one of the most important and commonly used antimicrobial agents that constitute more than 50% of the prescribed antibiotics across the word [36]. Carbapenem resistance problem has become increased over a passage of time which can be attributed to several factors such as consumption of large dosages of these carbapenems, concurrent usages of other antibacterial classes, gaining of newer resistance markers and their spread among the bacteria through horizontal gene transfer [5]. More than 23,000 people die annually in USA only due to the infections caused by antibiotic-resistant organism, as reported by the Centers for Disease Control and Prevention [37]. Earlier studies have mainly focused on active-site residues[3,38,39]. While others have explored the method of the substrate enzyme catalytic mechanism on the non-active site residues [14,15]. However, critical analysis of the NDM-1 structure, which has revealed that the substitution of amino acid residues near active site, may also contribute significantly thus; a detailed biochemical and biophysical

View Article Online
DOI: 10.1039/C9CP02734C

investigation are needed. In this study we have chosen four mutants (N193A, S217A, G219A and T262A) of the NDM-1 to explored substrate enzyme catalytic mechanism. The wild type and all mutants were found overexpressed and subsequently purified, as previously reported [14,15]. These mutants have been generated by substituting asparagine, serine, glycine and threonine with alanine at position of 193, 217, 219 and 262, respectively to understand the role of these residues in coordination of zinc 1 and zinc 2 ions for stability of enzyme. The change in residues explains in these mutants to understand the importance of these residues in catalytic reactions. Presence of threonine (T), glycine (G), asparagine (N) and serine (S) residues near the omega-loop of serine beta-lactamases has been confirmed to confer hydrolytic reactions by insulating water molecules at the active site for the final deacylation reactions [5,11]. Previous studies have proved that the amino acid sequence found 32.4% sequence similarity among VIM-2 and NDM-1, and 28.7% identity between IMP-1 and NDM-1 [5]. To the best of our knowledge this is the first study to identify role of these residues in NDM-1, leading to loss of enzyme function. MIC was performed for ampicillin, imipenem, meropenem, cefotaxime, cefoxitin and ceftazidime to check the activity of the mutant as compared to wild type. Primarily we performed MIC, to know the minimum inhibitor concentration. MIC was reduced to 2 to 6 fold as compared to the wild type. Reduction of the MIC as compared to wild type exhibited that these mutants were less stable, hence proved that these were function loss mutants. Further, enzyme kinetics was carried out with ampicillin, imipenem, meropenem, cefotaxime, cefoxitin and ceftazidime drugs to explore hydrolysis mechanism. Enzyme kinetics data showed decreased in Kcat/Km values while increased in km values as compared to wild type. The affinity of the NDM-1^{N193A}, NDM-1^{S217A}, NDM-1^{T262A} and NDM-1^{G219A} were reduced considerably with all tested antibiotics due to replacement of residues N193(Polar), S217(Polar), G219 (Non-Polar) and T262(Polar)) with

View Article Online
DOI: 10.1039/C9CP02734C

Alanine (Hydrophobic nature) [40]. The half maximal inhibitory concentration (IC50) is a measure of the efficacy of a substance inhibiting a specific biological function. It was clearly found that IC50 values decreased as compared to the wild type with all the drugs. Consumption of the drug in lesser amount as compared to wild type showed less hydrolysis as shown in mutants (N193A, S217A, G219A and T262A). All mutant showed lower IC50 values and higher affinity with enzyme [41]. Results of structural modelling indicated that all mutant protein tertiary models showed better DOPE scores and similar energy profiles pattern with the wild type proteins. All protein models were optimized by MD simulation and observed that all models along with wild type showed stable and consistent behavior of RMSD, RMSF and Rg. Structure validation of all the protein models was accomplished by using different quality check tools. Initially, the models were validated through the inspection of phi/psi distribution by plotting in Ramachandran plot obtained from PROCHECK analysis using SAVES (Structure Analysis and Verification Server) server. Refined protein models were further used for molecular docking. Molecular docking was carried by using Autodock Vina software. Ala 121, His 122, Gln 123, Asp 124, Glu 152 and Asn220 are important residues of NDM and its mutants (G219A, N193A, S217A and T262A) in interaction with imipenem and meropenem [3]. All models were further optimized and best binding pose of each receptor-ligand complex was selected as input for MD simulation. MD simulation was used to refine and check the stability of protein models in dynamic system. The complexes of wild type, G219A, N193A, S217A and T262A bound to imipenem and meropenem drugs were selected as started conformation for MD simulation. MD simulation was carried out using GROMACS 5.0. Protein and ligand topologies were derived using GROMOS 53A3 force field and PRODRG sever [31]. Molecular dynamic simulation data is used to evaluate the binding stability of imipenem and meropenem against the NDM-1 and its mutants (N193A, S217A,

View Article Online
DOI: 10.1039/C9CP02734C

G219A and T262A). 50ns of molecular dynamics simulation studies were performed for each ligand bound NDM systems[42]. All protein-imipenem and -meropenem complexes exhibited similar behaviors of RMSD, RMSF and Rg with slight changes in some mutant-meopenem complexes. Results of secondary structure analysis showed that in most of the cases, secondary structure entities such as sheets and helices were altered in case of protein-drug complexes implying the stable conformation of proteins were achieved in the presence of both the drugs which was also observed during CD analysis. Both docking and binding free energy calculation from MD simulation suggested that almost all mutant protein complexes were having higher docking scores and binding free energies indicating stable mutant-drug complex. Stable conformations and higher binding free energies of mutant-drug complexes as compared with wild type provide evidence of drug resistant toward NDM proteins. Circular dichroism was used to determine the secondary structure. It was found altered due to the loss of intermolecular forces, responsible for maintaining the structure [24]. In our experiment α helical content was also found effected (20 to 40%) same as reported in the crystal structure of wild-type NDM-1 [25, 26]. A distorted far–UV CD spectrum along with a decreased α-helical content was observed for mutant enzymes, revealing significant structural changes as compared to NDM-1 (Figure 8).

5 Conclusions

We conclude that N193, S217, G219, and T262 play a significant role in arranging the proper orientation of the active site of NDM-1 and also participated considerably to the overall stability of the enzyme. Our study emphasized the need to further address the significance of the residues which are near to the active site to maintain the function of NDM-1. Hence, this study supports to understand the resistance mechanism of carbapenemase in enterobacterial species. Moreover,

View Article Online
DOI: 10.1039/C9CP02734C

it may also help to design mechanism based specific inhibitors to block the action of enzyme and could be proposed as effective future drug candidates.

Acknowledgements

The study was supported by ICMR grant, AMR/5/2011-ECD-1 and DBT Grant, BT/PR8281/BID/7/448/2013. Authors are thankful to Indian Council of Agricultural Research, Ministry of Agriculture and Farmers' Welfare, Govt. of India for providing financial assistance in the form of CABin grant (F.no.Agril. Edn.4-1/2013-A&P) as well as Advanced Super Computing Hub for Omics Knowledge in Agriculture (ASHOKA) facility at ICAR-IASRI, New Delhi, India.

Author Contributions

AA, performed experiments, written draft of manuscript; RK performed bioinformatic analysis and MD simulation. MAI, SJ, DK help in bioinformatic analysis; AUK, designed problem, analyze data and checked and edited manuscript, provided reagents and lab space.

Competing financial interests' statement

None to declare

References

1. WHO 2017.Critically Important Antimicrobials for Human Medicine: Ranking of Antimicrobial Agents for Risk Management of Antimicrobial Resistance due to Non-Human Use. Geneva : World Health Organization 2017.
2. Brown, D. Antibiotic resistance breakers: can repurposed drugs fill the antibiotic discovery void? Nat. Rev. Drug Discov. 2015.14, 821–832.

View Article Online
DOI: 10.1039/C9CP02734C

3. Sun Z, Hu L, Sankaran B, Prasad BVV, Palzkill T. Differential active site requirements for NDM-1 β-lactamase hydrolysis of carbapenem versus penicillin and cephalosporin antibiotics. Nat Commun Oct 2018. 30;9(1):4524.
4. Grover CN, Sahni BAK, Bhattacharya CS. Therapeutic challenges of ESBLs and AmpC β-1 lactamase producers in a tertiary care center. Med J Armed Forces India. Jan; 2013. 69(1):4-10.
5. Kashyap A, Gupta R, Sharma R, Verma VV, Gupta S, Goyal P. New Delhi Metallo Beta Lactamase : Menace and its Challenges. J Mol GenetMed 2017, 11: 299.
6. Palzkill T. Metallo-β-lactamase structure and function. Ann NY Acad Sci.2013 1277:91–104.
7. Kumar R, Maurya R, Saran S. Identification of novel inhibitors of the translationally controlled tumor protein (TCTP): insights from molecular dynamics. Mol BioSyst 2017, 13:510-524.
8. Makena A, Brem J, Pfeffer I, Geffen RE, Wilkins SE, Tarhonskaya H, Flashman E, Phee LM, Wareham DW, Schofield CJ. Biochemical characterization of New Delhi metallo-β-lactamase variants reveals differences in protein stability. J Antimicrob Chemother 2015, 70:463.
9. Kumarasamy KK, Toleman MA, Walsh TR, Bagaria J, Butt F, Balakrishnan R, Chaudhary U, Doumith M, Giske CG, Irfan S, Krishnan P, Kumar AV, Maharjan S, Mushtaq S, Noorie T, Paterson DL, Pearson A, Perry C, Pike R, Rao B, Ray U, Sarma JB, Sharma M, Sheridan E, Thirunarayan MA, Turton J, Upadhyay S, Warner M, Welfare W, Livermore DM, Woodford N. Emergence of a new antibiotic resistance

View Article Online
DOI: 10.1039/C9CP02734C

mechanism in India, Pakistan, and the UK: a molecular, biological, and epidemiological study.Lancet 2010, 10:597–602.

10. Nordmann P, Poirel L, Toleman MA, Walsh TR. Does broad-spectrum β- lactam resistance due to NDM-1 herald the end of the antibiotic era for treatment of infections caused by Gram-negative bacteria? J Antimicrob Chemother 2011. 66:689–92.
11. Delaire M, Lenfant F, Labia R, Masson JM. Site-directed mutagenesis on TEM-1 ß-lactamase : role of Glul66 in catalysis and substrate binding. Protein Eng 1991.4:805–10.
12. Vakulenko SB, Tóth M, Taibi P, Mobashery S, Lerner SA. Effects of Asp-179 mutations in TEMpUC19 beta lactamase on susceptibility to betalactams. Antimicrob Agents Ch 1995. 39:1878–80.
13. Cunningham BC, Wells JA. High-resolution epitope mapping of hGH-receptor interactions by alanine-scanning mutagenesis. Science 1989. Jun 2;244(4908):1081-5.
14. Ali A, Azam MW, Khan AU. Non-active site mutation (Q123A) in New Delhi metallo-β-lactamase (NDM-1) enhanced its enzyme activity. Int J Biol Macromol. 2018.112:1272-1277.
15. Ali A, Gupta D, Khan AU. Role of non-active site residues in maintaining New Delhi metallo-β-lactamase-1(NDM-1) function: an approach of site directed mutagenesis and docking. FEMS Microbiol Lett. 2019 Jan 9. doi: 10.1093/femsle/fnz003.
16. Wayne, PA. Clinical and Laboratory Standards Institute.Performance standards for antimicrobial susceptibility testing: 21st informational supplement , 2014. M100-S24. CLSI.

View Article Online
DOI: 10.1039/C9CP02734C

17. Khan AU, Ali A, Danishuddin, Srivastava G, Sharma A. Potential inhibitors designed against NDM-1 type metallo-β-lactamases: an attempt to enhance efficacies of antibiotics against multi-drug-resistant bacteria. Sci Rep. Aug 23; 2017.7(1):9207.

18. Rose PW, Beran B, Bi C, Bluhm WF, Dimitropoulos D, Goodsell DS, Prlic A, Quesada M, Quinn GB, Westbrook JD, Young J. The RCSB Protein Data Bank: redesigned web site and web services. Nucleic Acids Res. 2010. 39:D392-D401.

19. Feng, Han, Xuehui Liu, Sheng Wang, Joy Fleming, Da-Cheng Wang, and Wei Liu. The mechanism of NDM-1-catalyzed carbapenem hydrolysis is distinct from that of penicillin or cephalosporin hydrolysis. Nat Commun. 2017. 8 (1): 2242.

20. Fiser A, Sali A. Modeller: generation and refinement of homology-based protein structure models. Methods Enzymol 2003. 374:461-491.

21. Van Der Spoel D, Lindahl E, Hess B, Groenhof G, Mark AE, Berendsen HJ. GROMACS: fast, flexible, and free. J. Comput Chem. 2005. 26(16):1701-1718.

22. J. A. Lemkul, W. J. Allen, D. R. Bevan. Practical considerations for building GROMOS compatible small-molecule topologies, J. Chem. Inf. Model 2010.50, 2221–2235.

23. Hess B, Bekker H, Berendsen HJ, Fraaije JG . LINCS: a linear constraint solver for molecular simulations. J Comput Chem 1997. 18:1463-1472.

24. Laskowski RA, MacArthur MW, Moss DS, Thornton JM. PROCHECK . A program to check the stereochemical quality of protein structures. J App Crystallogr 1993, 6:283-291.

25. Luthy R, Bowie JU, Eisenberg D. Assessment of protein models with three-dimensional profiles. Nature 1992, 356:83.

View Article Online
DOI: 10.1039/C9CP02734C

26. Wiederstein M, Sippl MJ. ProSA-web .Interactive web service for the recognition of errors in three-dimensional structures of proteins. Nucleic Acids Res 2007, 35:407-410.

27. Trott O, Olson AJ . AutoDock Vina: improving the speed and accuracy of docking with a new scoring function, efficient optimization, and multithreading. J Comput Chem 2010. 31: 455-461.

28. Wishart, David S., Yannick D . Feunang, An C. Guo, Elvis J. Lo, Ana Marcu, Jason R. Grant, Tanvir Sajed et al. DrugBank 5.0: a major update to the DrugBank database for 2018. Nucleic acids research 2017, 46, no. D1 : D1074-D1082.

29. N. M. O'Boyle, M. Banck, C. A. James, C. Morley, T. Vandermeersch, G. RHutchison . Open Babel: An open chemical toolbox, J. Cheminform., 2011. 3, 33.

30. Morris GM, Huey R, Lindstrom W, Sanner MF, Belew RK, Goodsell DS, Olson AJ. AutoDock4and AutoDockTools4: Automated docking with selective receptor flexibility. J Comput Chem 2009, 30:2785-2791.

31. Schuettelkopf AW,Van Aalten DM. PRODRG: a tool for high-throughput crystallography of protein–ligand complexes. Acta Crystallogr D Biol Crystallogr 2004, 60:1355-1363.

32. Kumari R, Kumar R, Open Source Drug Discovery Consortium, Lynn A. g_mmpbsaA GROMACS tool for high-throughput MM-PBSA calculations. J Chem Inf Model 2014, 54:1951-1962.

33. Wallace AC, Laskowski RA, Thornton JM. LIGPLOT: a program to generate schematic diagrams of protein-ligand interactions. Protein Eng Des and Sel 1995, 8:127-13

View Article Online
DOI: 10.1039/C9CP02734C

34. Raval A, Piana S, Eastwood MP, Dror RO, Shaw DE. Refinement of protein structure homology models via long, all-atom molecular dynamics simulations. Proteins 2012, ,80:2071-2079.

35. Heitz F, Van Mau N. Protein structural changes induced by their uptake at interfaces. Biochim Biophys Acta 2002.1597:1-1.

36. Drawz, S. M.; Bonomo, R. A . Three decades of β-lactamase inhibitors. Clin. Microbiol. Rev. 2010, 23, 160−201.

37. Antibiotic Resistance Threats in the United States. Centers for Disease Control and Prevention. 2013 Downloaded from http://www.cdc.gov/drugresistance/threat-report-2013/index.html, last accessed on March 9, 2015.

38. Kim Y, Cunningham MA, Mire J, Tesar C, Sacchettini J, Joachimiak A . NDM-1, the ultimate promiscuous enzyme: substrate recognition and catalytic mechanism. FASEB J 2013. 27: 1917-1927.

39. Zhu K, Lu J, Liang Z, Kong X, Ye F, Jin L, Geng H, Chen Y, Zheng M, Jiang H, Li JQ, Luo C. A quantum mechanics/ molecular mechanics study on the hydrolysis mechanism of New Delhi metallob-lactamase-1. J Comput Aid Mol Des; 27: 247–256. J Comput Aided Mol Des. 2013, 27(3):247-56.

40. Yan BX, Sun YQ. Glycine residues provide flexibility for enzyme active sites. J Biol Chem. 1997 Feb 7;272(6):3190-4.

41. Khan A, Faheem M, Danishuddin M, Khan AU. Evaluation of inhibitory action of novel non β-lactam inhibitor against Klebsiella pneumoniae carbapenemase (KPC-2). PLoS One. 2014 Sep 29;9(9):e108246.

View Article Online
DOI: 10.1039/C9CP02734C

42. Ali A, Gupta D, Srivastava G, Sharma A, Khan AU . Molecular and computational approaches to understand resistance of New Delhi Metallo β- lactamase variants (NDM-1, NDM-4, NDM-5, NDM-6, NDM-7)-producing strains against carbapenems. J Biomol Struct Dyn 2018. May 11,2018:1-40.

FIGURE LEGENDS

Figure 1: Alignment sequence of IMP, NDM-1, NDM-4, VIM-4 and VIM-2 were performed using online softwere Clustal Omega 2. The conserved sequence of NDM-1 residues (N193, S217,G219 and T262) are highlighted with yellow colour. All residues are levelled according to NDM-1 sequences.

Figure 2: Superimposition of three dimensional models of NDM-1, IMP 1 and VIM-1. The enzyme-active sites and target residues under investigation are shown as sticks and highlighted in red circle and black square boxes, respectively. Protein structures and residues of NDM-1 have been shown in green color, IMP-1 in blue and VIM-1 in yellow colors, respectively. 3D structure is rendered in PyMOL graphical system.

Figure 3: Determination of the IC50 values with selected drug imipenem, meropenem, cefotaxime, cefoxitin and ceftazidime with residual activity of NDM-1 and its mutants as monitored by the hydrolysis with constant value of 100 μM nitrocefin (A) IC50 of NDM-1 (B) N193A (C) S217A (D) G219A (E) N262A.

Figure 4: MD simulation of different protein models**.** (A) Energy (kJ/mol) of different system, (B) Root mean square deviation (RMSD) in nanometer with respect to time, (C) Root mean square fluctuation (RMSF) in nanometer with respect to amino acid residues, and (D) Radius of gyration in nanometer with respect to time. Wildtype, G219A, N193A, S217A and T262A were

View Article Online
DOI: 10.1039/C9CP02734C

shown in black, blue, red, green and yellow colors, respectively. All simulation was run for 50 ns of production run. Black dotted circles represented the amino acids residue with higher mobility.

Figure 5: RMSD of all proteins-imipenem and meropenem complexes. (A) RMSD of different receptors with imipenem drugs with respect to time, (B) RMSD of imipenem drug complexed with different receptors with respect to time, (C) RMSD of different receptors with meropenem drugs with respect to time and (D) RMSD of meropenem drug complexed with different receptors with respect to time. Wildtype, G219A, N193A, S217A and T262A were shown in black, blue, red, green and yellow colors, respectively.

Figure 6: RMSF and Rg of all proteins-imipenem and meropenem complexes. (A) RMSF of different receptors with imipenem drugs with respect to amino acids residues, (B) Radius of gyration in nanometer of different receptors complexed with imipenem drug with respect to time, (C) RMSF of different receptors with meropenem drugs with respect to amino acids residues and (D) Radius of gyration in nanometer of different receptors complexed with meropenem drug with respect to time . Wildtype, G219A, N193A, S217A and T262A were shown in black, blue, red, green and yellow colors, respectively. Black dotted circles represented the amino acids residue with higher mobility.

Figure 7: Secondary structures formation in absence and presence of imipenem and meropenem drugs. (A) Percentage of secondary structure formation of wildtype and mutant proteins in absence and presence of imipenem drug, and (B) Percentage of secondary structure formation of wildtype and mutant proteins in absence and presence of meropenem drug. Coil, β-sheets, bend, turn and α-helices were represented in black, red, grey, green and blue colours, respectively.

View Article Online
DOI: 10.1039/C9CP02734C

Figure 8: Far UV-CD spectra of NDM-1^{G219A}, NDM-1^{N193A}, NDM-1^{S217A} and NDM-1^{T262A} mutants, compared with wild type NDM-1. Spectra were obtained at 28°C in 50 mM HEPES buffer.

Table 1: MICs of *bla*$_{NDM-1}$ ^{G219A}, *bla*$_{NDM-1}$ ^{N193A}, *bla*$_{NDM-1}$^{S217A} and *bla*$_{NDM-1}$ ^{T262A} mutants, compared with wild-type NDM-1 clone for different antibiotics.

MIC on *E. coli* DH5α (mg/liter)						
Antibiotics	**Wild-type NDM-1**	**G219A Mutant**	**N193A Mutant**	**S217A Mutant**	**T262A Mutants**	**pQE-2 (vector only)**
Ampicillin	1024	1024	1024	1024	1024	**1024**
Imipenem	128	32	32	64	32	0.5
Meropenem	64	8	4	32	2	0.5
Cefotaxime	32	32	32	64	32	0.5
Cefoxitin	32	512	32	512	512	0.5
Ceftazidime	16	8	8	16	8	0.5
Aztreonam	ND	ND	ND	ND	ND	ND

*Ampicillin resistance marker already present in PQE-2 vector as a selection marker.

Table 2: IC50 values for the NDM-1and all mutant $_{NDM-1}^{N193A}$, $_{NDM-1}^{S217A}$, $_{NDM-1}^{G219A}$ and $_{NDM-1}^{T262}$ with imipenem, meropenem, cefotaxime, cefoxitin and ceftazidime.

IC50 (μM) values										
	Imipenem	**% Reduced**	**Meropenem**	**% Reduction**	**Cefotaxime**	**% Reduction**	**Cefoxitin**	**% Reduction**	**Ceftazidime**	**% Reduction**
NDM-1	**2.8641**	**100 %**	**2.3350**	**100 %**	**2.4323**	**100%**	**2.7671**	**100 %**	**2.5649**	**100 %**

View Article Online
DOI: 10.1039/C9CP02734C

N193A	**1.4450**	**50%**	**2.2412**	**95%**	**1.7871**	**73%**	**1.1972**	**43%**	**1.4512**	**56%**
S217A	**2.2642**	**79%**	**2.2093**	**94%**	**1.4340**	**58%**	**1.6830**	**66%**	**1.5341**	**59%**
G219A	**2.5754**	**89%**	**2.2610**	**96%**	**1.9601**	**80%**	**2.5442**	**91%**	**2.2662**	**88%**
T262A	**1.7291**	**60%**	**1.9991**	**85%**	**2.2472**	**92%**	**1.5241**	**55%**	**1.3521**	**52%**

Table 3: Steady-state enzyme kinetics of wild-type NDM-1enzyme and NDM-1^{G219A}, NDM-$1^{N193A,}$ NDM-1^{S217A} and NDM-1^{T262A} mutants' enzyme.

	Wild Type NDM-1			G219A			N193A			S217A			T262A		
	Km (μM)	Kcat(s^{-1})	Kcat / Km($\mu M^{-1}S^{-1}$)	Km (μM)	Kcat(s^{-1})	Kcat / Km($\mu M^{-1}S^{-1}$)	Km (μM)	Kcat(s^{-1})	Kcat / Km($\mu M^{-1}S^{-1}$)	Km (μM)	Kcat(s^{-1})	Kcat / Km($\mu M^{-1}S^{-1}$)	Km(μM)	Kcat(s^{-1})	Kcat / Km($\mu M^{-1}S^{-1}$)
Nitrocefin	27.3021±0.4492	118.6234±0.4617	4.3440±1.027	247.3211±2.543	30.3921±0.2411	0.1228±0.094	105.8701±8.136	13.0932±0.1007	0.1245±0.012	54.0011±5.303	11.6798±0.3644	0.2161±0.068	29.4542±0.3600	9.5402±2.661	0.3229±7.391
Ampicillin	22.9632±4.53	103.332±5.500	4.5101±1.211	147.1213±11.18	19.7098±0.7634	0.1339±0.0681	36.9523±1.280	7.1061±0.4568	0.1923±0.3568	59.2132±2.696	849.07621±0.1431	14.3376±0.0530	67.0921±3.486	65.5576±0.2599	0.9770±0.040
Cefotaxime	63.8223±8.013	141.6543±0.4944	2.2182±0.0616	87.5454±2.855	15.2287±0.2007	0.1738±0.0702	110.3097±1.002	14.3234±0.6372	0.1298±0.6359	80.8554±1.654	96.2309±0.6543	1.1906±0.3955	80.9576±1.078	63.8843±7.405	0.7891±6.869
Cefoxitin	45.7356±6.031	134.734±0.4107	2.9451±0.0680	68.8347±1.935	16.2374±0.1795	0.2430±0.0927	49.2809±2.423	7.9440±0.1306	0.1612±0.0543	56.1900±4.393	11.4311±0.3036	0.2034±0.0693	70.9709±1.2532	7.3842±1.252	0.1040±0.9991
Ceftazidime	51.5123±3.398	106.1098±0.1398	2.0592±0.0411	73.1451±5.947	15.2093±0.4591	0.2083±0.0771	64.9400±4.551	10.0223±0.2561	0.1542±0.0562	82.1632±2.023	19.0117±0.1153	0.2333±0.0569	53.3098±1.181	7.5701±0.5298	0.1480±0.4486
Imipenem	66.5800±4.756	121.1001±0.2295	1.8181±0.0482	106.9234±4.448	92.0039±0.1642	0.8642±0.036	224.8234±9.265	26.0621±0.1391	0.1159±0.0150	119.0213±6.639	135.3213±0.366	1.1360±0.0551	155.3±2.096	10.3300±0.8659	0.0665±0.4131
Meropenem	60.7611±4.490	144.8661±0.1174	2.3831±0.0261	63.5601±4.68	15.3433±0.5409	0.2413±0.1158	66.7600±1.604	10.9311±7.522	0.1637±4.689	102.1226±3.524	52.5800±0.2251	0.5124±0.0631	107.1023±4.909	12.0221±0.2437	0.1113±0.4964

View Article Online
DOI: 10.1039/C9CP02734C

Aztreonam	ND	ND	ND	ND	ND	ND	ND	ND	ND	ND	ND	ND	ND	ND	ND

Table 4: Docking scores of protein-ligand complexes (Docking score is expressed in ΔE)

Proteins	Imipenem	Meropenem
Wildtype	-5.9	-7.1
G219A	-5.7	-7.1
N193A	-5.7	-7
S217A	-5.8	-7
T262A	-5.9	-7

Table 5: Binding free energy for wildtype- and mutant-imipenem complex. (ΔG is expressed in kcal/mol)

	vander waal energy	STV	Electrostatic energy	STV	Polar solvation energy	STV	SASA energy	STV	Binding energy (ΔG)	STV
Wildtype	-64.7262	±11.4011	-2.0540	±1.3111	33.6951	±3.6234	-8.2512	±1.4210	-41.5091	±13.5210
G219A	-104.4810	± 7.6091	-3.8421	±0.8987	34.8812	±3.9011	-12.2890	±1.0623	-85.530	± 8.2098
N193A	-100.3771	± 2.7434	-1.8179	±1.3234	21.9251	±2.6213	-11.6132	±0.3021	-91.8432	± 2.5210
S217A	-70.8424	±12.1091	-3.0782	±0.7126	23.8632	±3.9021	-7.4961	±1.4231	-57.0182	±12.5129
T262A	-25.8772	±11.7012	-1.7732	±0.8097	22.8861	±7.7102	-2.8910	±1.3890	-7.6601	±12.5021

Table 6: Binding free energy for wildtype- and mutant-meropenem complex. (ΔG is expressed in kcal/mol).

	vander waal energy	STV	Electrostatic energy	STV	Polar solvation energy	STV	SASA energy	STV	Binding energy (ΔG)	STV
Wildtype	-133.305	± 7.29	-12.908	± 1.6	52.441	± 4.1	-13.98	± 0.8	-108.025	± 7.9
G219A	-113.925	± 14.4	-10.319	± 2.1	45.189	± 5.6	- 12.551	± 1.5	-91.735	± 12.9

View Article Online
DOI: 10.1039/C9CP02734C

N193A	-64.023	± 13.1	0.168	± 0.8	23.295	± 7.0	-7.658	± 1.4	-48.468	± 11.7
S217A	-107.628	± 13.4	-0.511	± 0.5	22.536	± 3.7	-10.635	± 1.3	-96.577	± 11.7
T262A	-130.878	± 11.8	-9.63	± 1.3	44.223	± 3.1	-13.499	± 1.0	-109.663	± 12.0

Figure 1

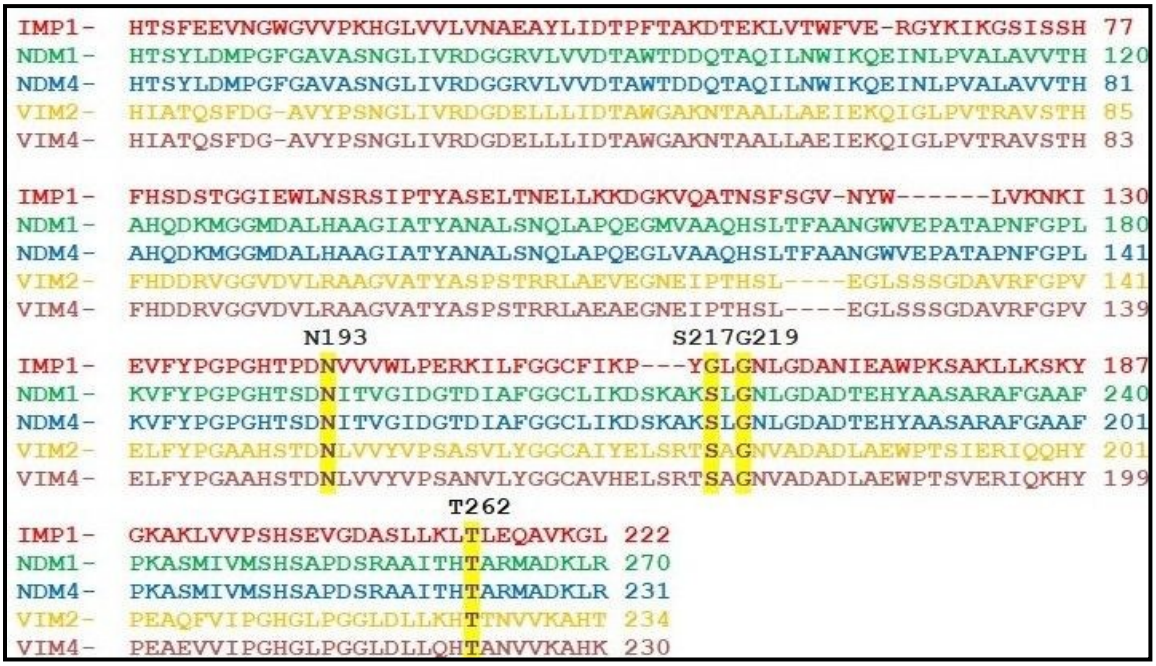

View Article Online
DOI: 10.1039/C9CP02734C

Figure 2

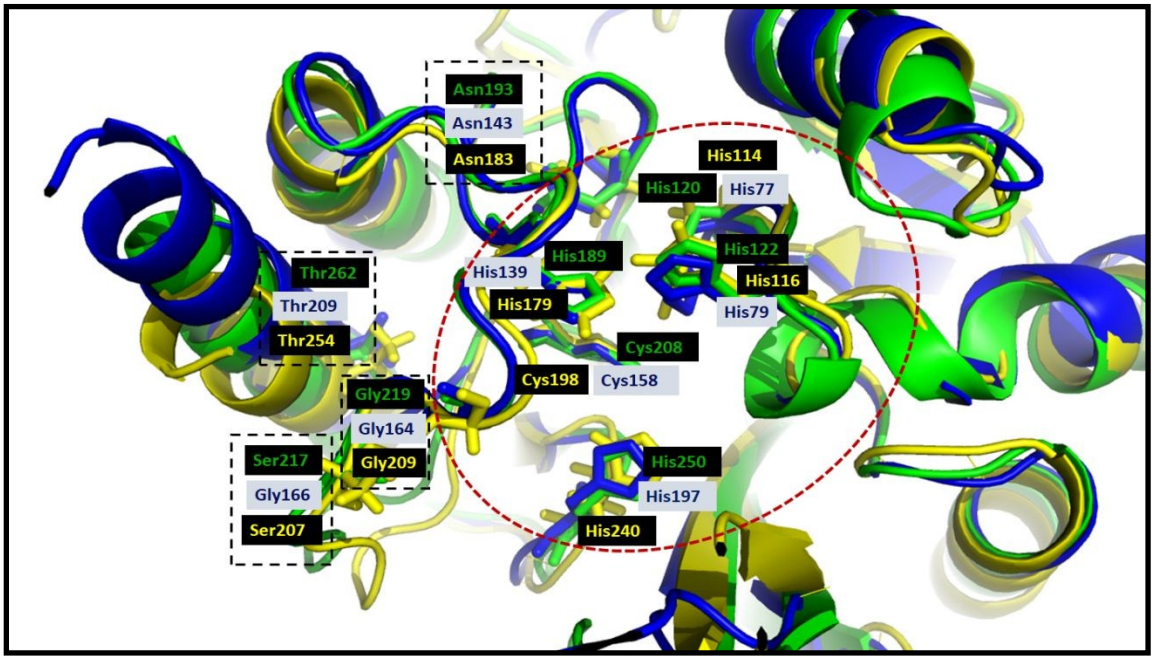

View Article Online
DOI: 10.1039/C9CP02734C

Figure 3

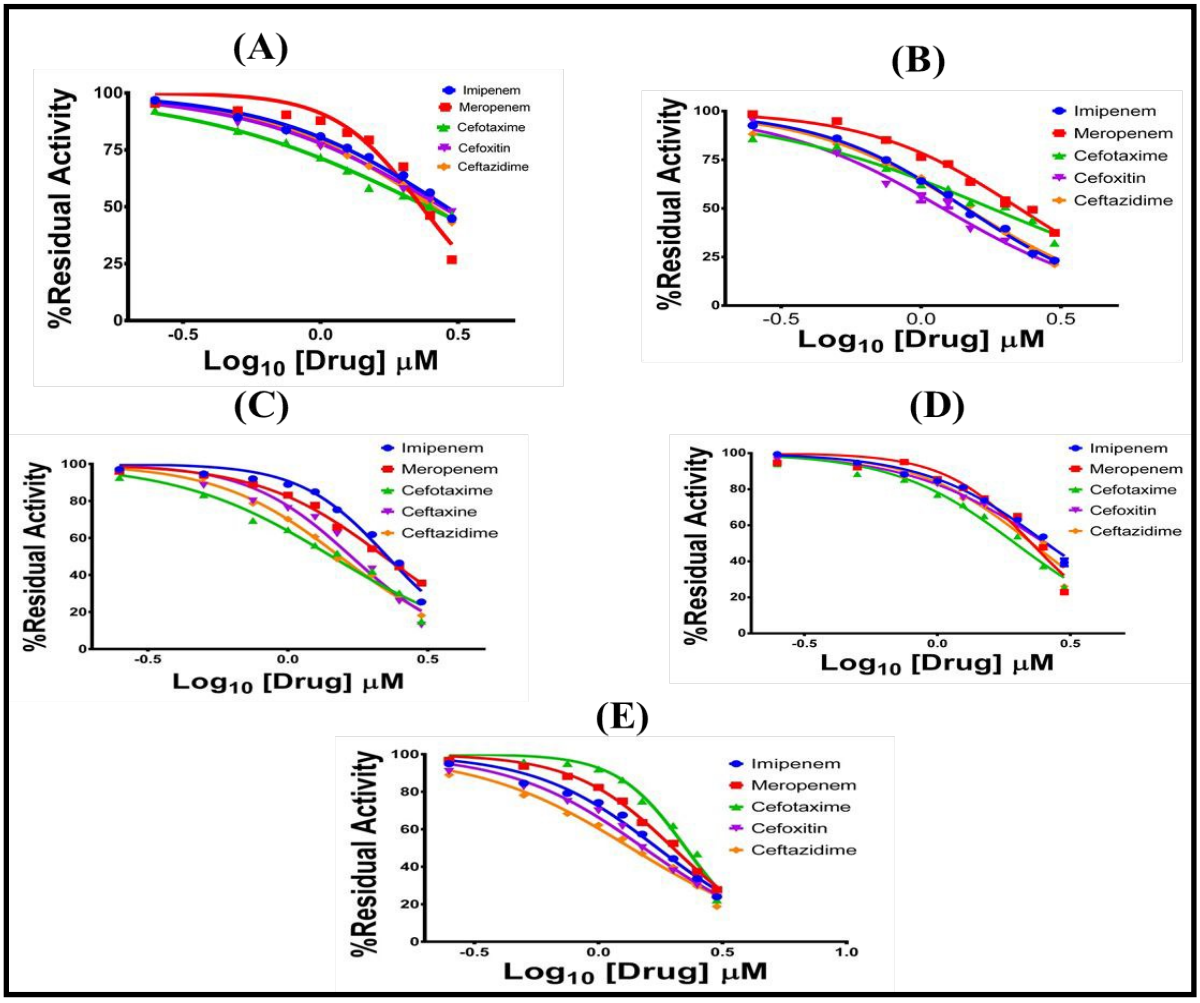

View Article Online
DOI: 10.1039/C9CP02734C

Figure 4

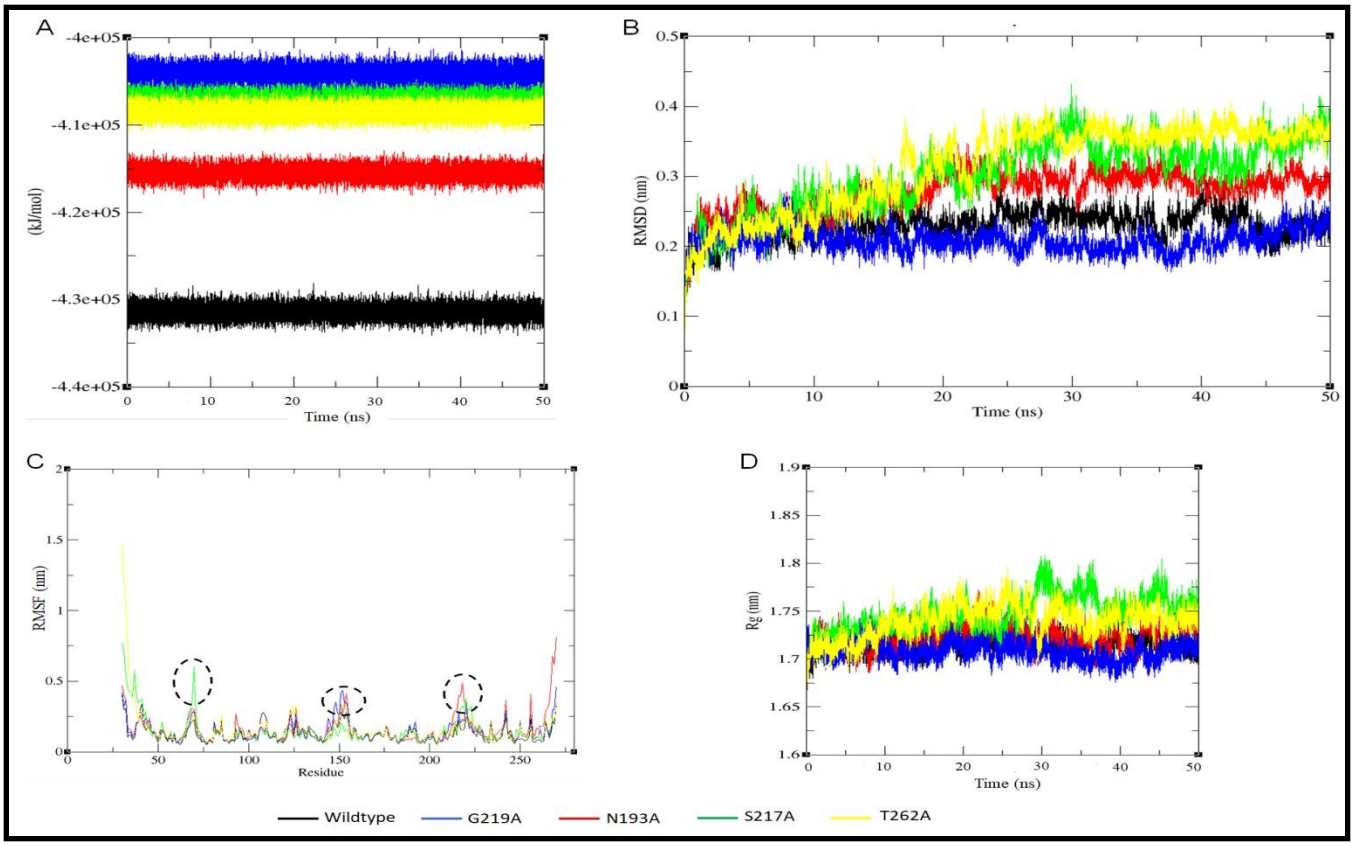

View Article Online
DOI: 10.1039/C9CP02734C

Figure 5

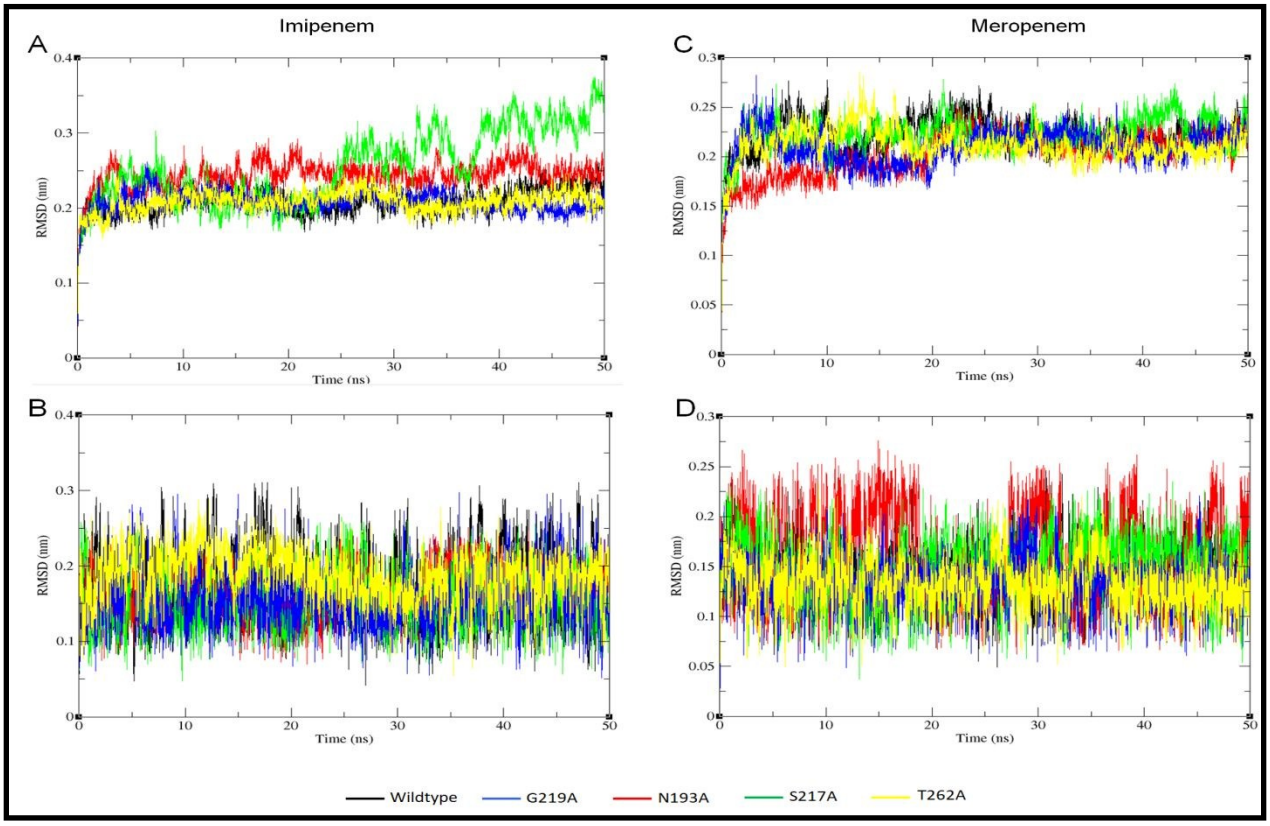

View Article Online
DOI: 10.1039/C9CP02734C

Figure.6

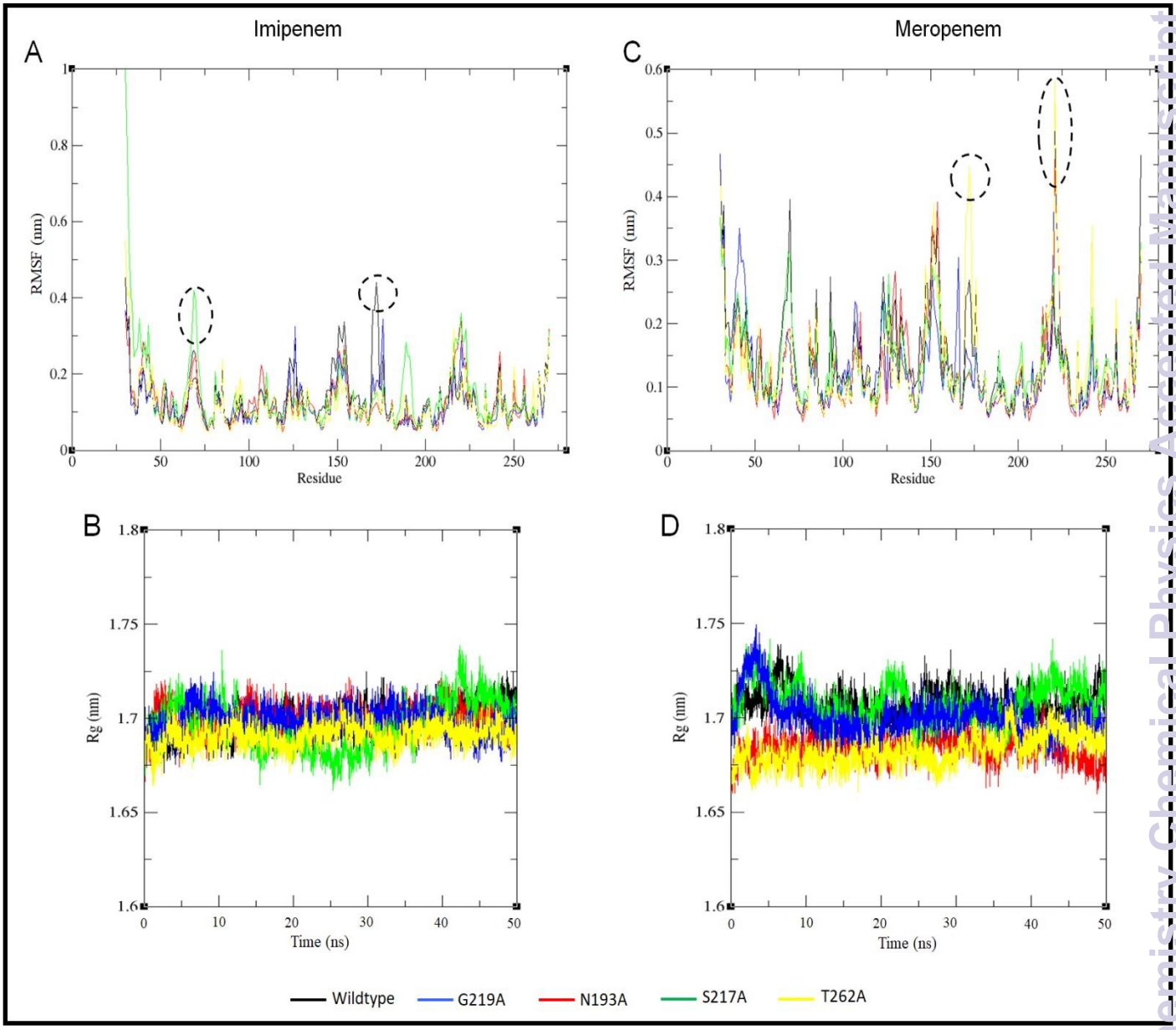

View Article Online
DOI: 10.1039/C9CP02734C

Figure.7

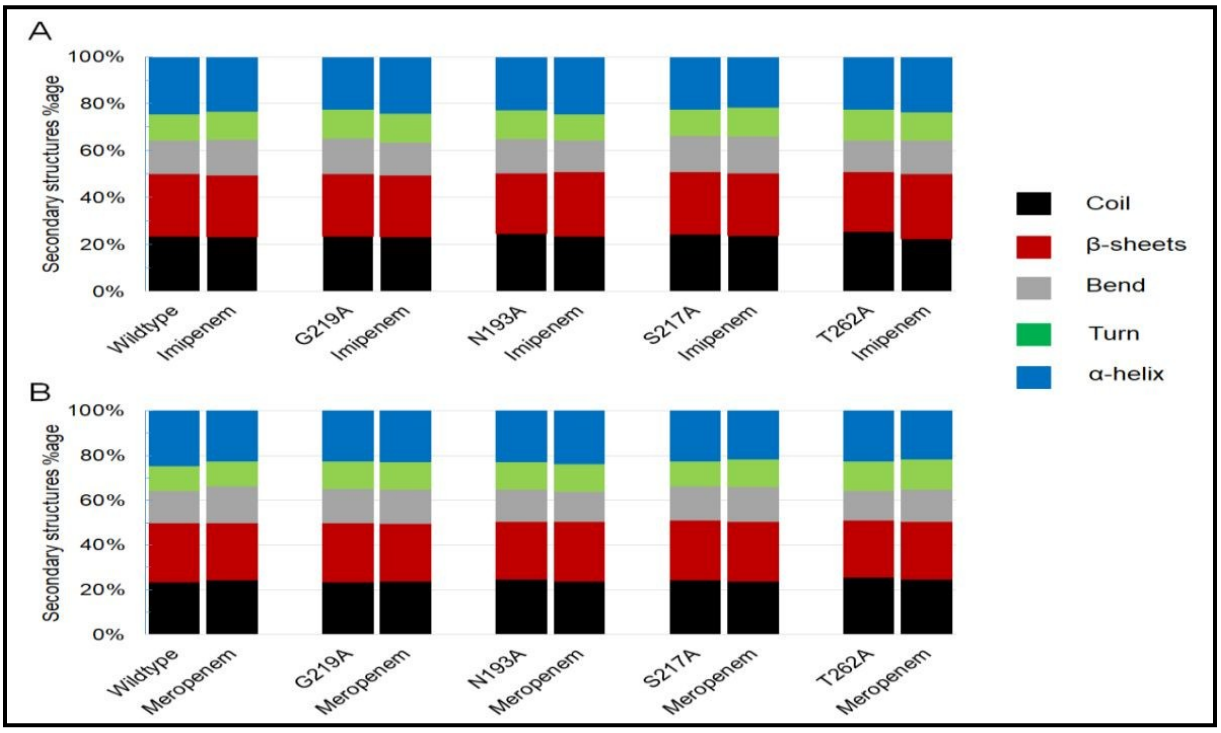

Figure 8.